2025 IEEE/SICE International Symposium on System Integration (SII)
January 21-24, 2025, Munich, Germany

Dynamic knitting simulation for predicting defects of knitted fabrics

Kazuki Hayano, Hidefumi Wakamatsu, Yoshiharu Iwata, and Yuya Yamada

***Abstract*— Knit products are widely used in people's daily lives because of their high functionality. Most such knit products are usually made of flat knitted fabric, which is the basic structure of knitted fabrics, and this unique structure of flat knitting gives knit products high functionality. However, a defect called *Yotari* often occurs during the creation of flat knitting. Since it impairs appearance and functionality of knit products, knit products must be knitted in such a way that it does not occur. However, the mechanism of it has not been theoretically elucidated, and there is a need to predict the occurrence of the problem and to investigate its causes. The purpose of this research is to predict the occurrence and determine the cause of it by dynamically analyzing yarns knitted on a knitting machine. In this paper, the hypothesis of the cause of it is verified. First, yarn is modeled based on its mechanical properties. Next, contact and friction that occur during knitting process are formulated. Finally, knitting process using a knitting machine is dynamically simulated to test the hypotheses of it.**

I. Introduction

Knit products are widely used in people's daily lives, such as sweaters and socks, because they are comfortable to wear due to their excellent elasticity and heat retaining properties [1]. Most such knit products usually consist of flat knitted fabric, which is the basic structure of knitted fabric. Flat-knit fabrics have structure of looped yarns strung together horizontally and vertically, and their unique structure makes the fabric thin and highly elastic in the horizontal direction. This is why it is often used in knit products [2]. However, when flat-knitted fabrics are made, a defect called *Yotari* (Figure 1), in which the loops tilt alternately to the left and right at each step, often occurs. Since it detracts from the appearance and functionality of knit products, knit products must be knitted in such a way that it does not occur. However, the mechanism of it has not been theoretically elucidated, and the presence or absence of it is not known until the actual knitting process. Therefore, in the modern knit product manufacturing process, when it occurs, it is easy for the knitting process to be reworked or the defect to be corrected, resulting in a serious problem of inefficiency and waste of yarns. Therefore, there is a need to predict the occurrence and investigate the cause of the problem in order to improve the productivity of knit products and to save resources.

Next, a hypothesis for the occurrence of Yotari in the current situation is discussed based on experimental results (Figure 2). Flat knitting fabrics are generally created by knitting yarn supplied from carriers that move alternately to the left and right. The half-loop on the carrier's direction-of-travel side has a larger amount of yarn supplied, resulting in a shrunken loop. In contrast, the half loop on the opposite side of the direction of travel has a smaller amount of yarn supplied

Kazuki Hayano, Hidefumi Wakamatsu, and Yoshiharu Iwata are with Dept. of Materials and Manufacturing Science, Graduate School of Eng., Osaka University, Yamadaoka 2-1, Suita, Osaka 565-0871, Japan.
e-mail: {kazuki.hayano, wakamatu, iwata} @mapse.eng.osaka-u.ac.jp

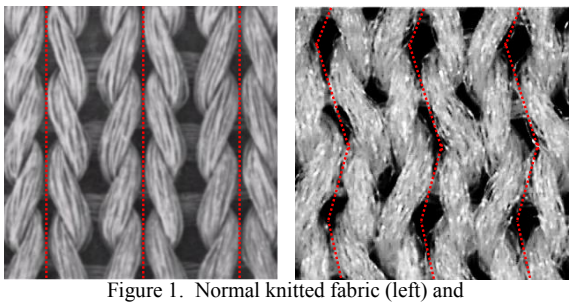

Figure 1. Normal knitted fabric (left) and knitted fabric that have defect "Yotari" (right).

and the loop is relatively stretched. The loop is fixed by friction with the loop one step below. If the friction between the yarns is high, the loop remains in the same shape as it was knitted. However, if the friction between yarns is small, the loops may be asymmetrical in shape due to the equalization of the elastic strain of the different yarns. In fact, experiments have shown that Yotari occurs significantly when the friction coefficient of yarns is small. Based on the above, the final goal of this research is to predict the occurrence and to determine the cause of it. In this paper, which is a preliminary verification, it is dynamically simulated yarn being knitted by a knitting machine based on modeling of yarn, and verify that an asymmetric distribution of normal strain is generated for loops.

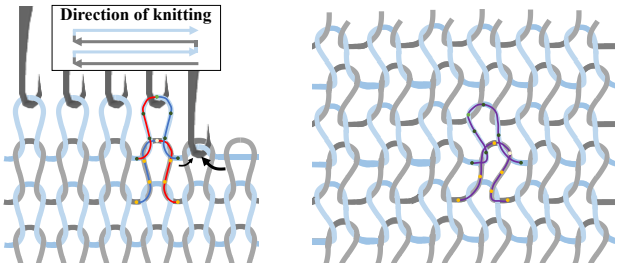

Figure 2. Hypothesis that Yotari occurs.

II. Previous Research

Much work has been done on predicting knitted fabrics. Jonathan modeled loops with B-spline curves and derived knitted fabrics formed by a variety of knitting techniques [3]. Cem simulated knitting by assigning knitted fabrics over a stitch mesh [4]. These models take as input an already created knitting topography and predict how the knitting topography will deform when the knitted fabric is subjected to force. This makes it impossible to predict the shape of a knitted fabric based on the state of the yarn. Thus, for predicting Yotari, it is needed to model yarn, which is material of knit fabrics, as well as a knitting machine, so that the effect of a knitting machine can be considered in the simulation. In this research, yarn and a knitting machine are modeled based mechanical properties.

Yuya Yamada is with SHIMA SEIKI MFG., LTD.; 85 Sakata, Wakayama 641-8511, Japan.
e-mail: y-yamada.6012@shimaseiki.co.jp

III. MODELING OF YARN

To perform a knitting simulation, yarn must be modeled. We have proposed a modeling method for yarn [5]. Let us briefly explain our modeling. There are three assumptions in the modeling. Firstly, yarn is discretely represented by a finite number of mass points connected by straight springs. Secondly, yarn is not deformed in the radial direction and the cross-sectional shape of yarn is always circular. Thirdly, mechanical properties, such as expanding/contracting, bending, and torsional deformation are considered. Based on those assumptions, yarn is modeled. If the length is L, yarn is represented by n mass points and $(n-1)$ straight springs directly connecting them. The position of each mass point is represented by the spatial coordinate system $O-xyz$. The expanding/contracting and bending deformation are expressed by displacement in the system. The expanding/contracting deformation is formulated by their force corresponding to the vertical displacement of straight springs (Figure 3(a)). The bending deformation is formulated by introducing a virtual bending spring on each mass point and bending force depends on the bending angle calculated from the position of the straight springs on both sides of the mass point (Figure 3(b)).

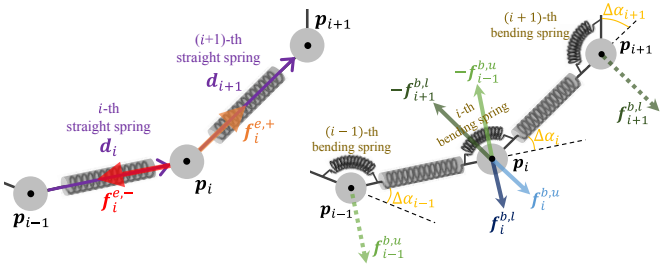

(a) expanding/contracting force (b) bending force

Figure 3. Deforming force in spatial coordinate system.

Next, the torsional deformation of yarn is formulated. Since the torsion of yarn cannot be represented by the spatial coordinate system alone, a new coordinate system is needed to represent the torsion. Therefore, the object coordinate system $P_i-\xi_i\eta_i\zeta_i$ is set for each mass point (Figure 4(a)). Note that the system is expressed by $\boldsymbol{q}_i=[q_{0,i}\quad q_{1,i}\quad q_{2,i}\quad q_{3,i}]^{\mathrm{T}}$ called the quaternion, and $\boldsymbol{q}_i$ must satisfy (1) by mathematical definition.

$$q_{0,i}^2+q_{1,i}^2+q_{2,i}^2+q_{3,i}^2-1=0,\qquad \forall i \tag{1}$$

The new system is set up, but if it is exercised independently of the spatial coordinate system, the model loses consistency between position and orientation and does not move correctly as yarn. Thus, a constraint is introduced to connect those two coordinates. In this research, it is referred to as *the rotational constraint*. It constrains each mass point so that the ζ_i axis is always the same direction as the i-th straight spring vector $\boldsymbol{d}_i$.

$$\boldsymbol{d}_i\cdot\boldsymbol{\xi}_i=0,\qquad \boldsymbol{d}_i\cdot\boldsymbol{\eta}_i=0,\qquad \forall i \tag{2}$$

To satisfy the constraint, if the constraint force acting on the $(i-1)$-th mass point $\boldsymbol{p}_{i-1}$ is set to $-\boldsymbol{\lambda}_i$, the i-th mass point $\boldsymbol{p}_i$ is subjected to its reaction force $\boldsymbol{\lambda}_i$.

$$\boldsymbol{\lambda}_i=\lambda_{\xi,i}\boldsymbol{\xi}_i+\lambda_{\eta,i}\boldsymbol{\eta}_i \tag{3}$$

Note that since it is the constraint to change orientation of the ζ_i axis, no constraint force in the direction of the ζ_i axis is generated. The constraint moment $\boldsymbol{M}_i$ also arises due to $\boldsymbol{\lambda}_i$.

$$\boldsymbol{M}_i=(-\boldsymbol{d}_i)\times(-\boldsymbol{\lambda}_i)=\boldsymbol{d}_i\times\boldsymbol{\lambda}_i \tag{4}$$

After satisfying the constraints, torsional deformation of yarn is formulated (Figure 4(b)). The torsional deformation of yarn is expressed as a rotational motion of the masses by using the rotational moment around the central axis of the straight spring.

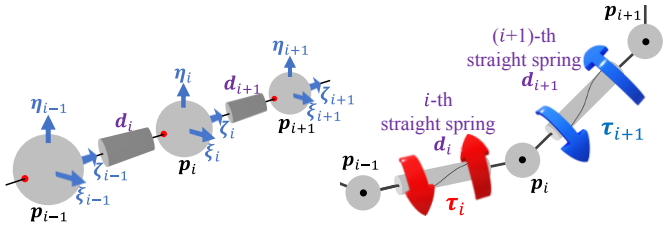

(a) an object coordinate $P_i-\xi_i\eta_i\zeta_i$ (b) torsional moments

Figure 4. Model diagram of an object coordinate and torsion.

Based on the above modeling of deformation, numerical analysis is described to predict shape of yarn. Let $\boldsymbol{f}_i^e$ be the expanding/contracting force from the straight springs connected to $\boldsymbol{p}_i$ and $\boldsymbol{f}_i^b$ be the bending force from the bending spring on $\boldsymbol{p}_i$. Also, let $\boldsymbol{\phi}_i$ be the torsional moments received from the straight springs connected to $\boldsymbol{p}_i$. Then, considering the terms related to the rotational constraint, the equations of motion for the translation and rotation of $\boldsymbol{p}_i$ can be formulated.

$$m\ddot{\boldsymbol{p}}_i-\boldsymbol{\lambda}_i=\boldsymbol{f}_i^e+\boldsymbol{f}_i^b \tag{5}$$

$$J\dot{\boldsymbol{\omega}}_i-\boldsymbol{M}_i=\boldsymbol{\phi}_i \tag{6}$$

Note that m is the mass of each mass point. J is the moment of inertia around each axis in the object coordinate, and $\dot{\boldsymbol{\omega}}_i$ is the angular acceleration around each axis. Since $\boldsymbol{\lambda}_i$ and $\boldsymbol{M}_i$ in the rotation constraint are forces and moments, they should originally be countable on the right-hand side of the equation of motion. However, since they are unknown, they are added to the left side of the equations of motion for convenience. From the above, the behavior of yarn is predicted by solving the differential equation using a numerical analysis method such as the Runge-Kutta method [6]. The constraints like (1) and (2) are considered using the constraint stabilization method [7]. The constraint equation to be introduced is set to $R=0$, and the following differential equation is formulated.

$$\ddot{R}+2\nu\dot{R}+\nu^2R=0 \tag{7}$$

This differential equation is solved simultaneously with the equations of motion such as (5) and (6), resulting in a simulation that includes constraints.

IV. FORMULATION OF CONTACT AND FRICTION

In this research, it is simulated that process of knitting yarn into fabric by a knitting machine to verify the asymmetry of normal strian of yarn, which is considered to be the cause of Yotari. Normal strian of yarn is considered to be caused by the drag of yarn on the surface of the needles in the process where yarn is strongly pulled in by the needles of a knitting machine (Figure 2). In other words, in order to verify the asymmetry of normal strain inside yarn by simulating knitted fabric, it is highly important to reproduce phenomena such as contact and friction that occur between yarn and a knitting machine. Also, since yarns are knitted while in contact and friction with other yarn, it is also necessary to reproduce contact and friction between yarn. Therefore, the formulation of contact and friction will be explained in this section.

A. *Contact and friction between yarn and a knitting machine*

Parts of a knitting machine that have a three-dimensional object shape are represented as a set of triangular meshes using STL (Standard Triangulated Language). Therefore, in order to model the contact and friction between yarn and a knitting machine, the contact and friction between components of the discrete model and the triangular mesh should be formulated.

A-1. A mass point and mesh surfaces

Let $\boldsymbol{v}_{1,j}$, $\boldsymbol{v}_{2,j}$ and $\boldsymbol{v}_{3,j}$ be the position vectors of the vertices of the j-th triangle mesh m_j, respectively, and let $\boldsymbol{e}_{1,j}$, $\boldsymbol{e}_{2,j}$ and $\boldsymbol{e}_{3,j}$ be the edge vectors in m_j. Also, let $\boldsymbol{n}_j$ be the outward normal vector at m_j. Let $\boldsymbol{p}_i^*$ be the coordinates of the projection of i-th mass point $\boldsymbol{p}_i$ onto m_j (Figure 5(a)).

$$\boldsymbol{p}_i^* = \boldsymbol{p}_i - \{\boldsymbol{n}_j \cdot (\boldsymbol{p}_i - \boldsymbol{v}_{1,j})\} \tag{8}$$

If $\boldsymbol{p}_i^*$ exists inside m_j, (9) is satisfied (Figure 5(b)). However, if it is not satisfied, then $\boldsymbol{p}_i^*$ exists outside of m_j (Figure 5(c)).

$$\begin{aligned}\mathrm{sgn}\{\boldsymbol{e}_{1,j} \times (\boldsymbol{p}_i^* - \boldsymbol{v}_{1,j}) \cdot \boldsymbol{n}_j\} + \mathrm{sgn}\{\boldsymbol{e}_{2,j} \times (\boldsymbol{p}_i^* - \boldsymbol{v}_{2,j}) \cdot \boldsymbol{n}_j\} \\ +\mathrm{sgn}\{\boldsymbol{e}_{3,j} \times (\boldsymbol{p}_i^* - \boldsymbol{v}_{3,j}) \cdot \boldsymbol{n}_j\} = 3\end{aligned} \tag{9}$$

If $\boldsymbol{p}_i$ satisfies the above equation and resides above or below m_j, the amount of penetration h_i is calculated by (10) using the radius r of the mass point.

$$h_i = r - \boldsymbol{n}_j \cdot (\boldsymbol{p}_i - \boldsymbol{p}_i^*) \tag{10}$$

The vertical drag force $\boldsymbol{F}_{Cv,i}$ acting on $\boldsymbol{p}_i$ between $\boldsymbol{p}_i$ and m_j can be formulated using the contact spring k_m (Figure 5(d)).

$$\boldsymbol{F}_{Cv,i} = k_m h_i \boldsymbol{n}_j \tag{11}$$

Next formulation is for frictional force resulting from contact. Suppose that $\boldsymbol{p}_i$ moves with a velocity $\boldsymbol{v}_{h,i,j}^{relative}$ to the tangential direction of m_j. In this case, the dynamic frictional force $\boldsymbol{F}_{Ch,i}$ acting on $\boldsymbol{p}_i$ is formulated using the coefficient of dynamic friction μ_d^m between yarn and a knitting machine.

$$\boldsymbol{F}_{Ch,i} = -\mu_d^m k_m h_i \frac{\boldsymbol{v}_{h,i,j}^{relative}}{|\boldsymbol{v}_{h,i,j}^{relative}|} \tag{12}$$

When dynamic friction force acts, the moment $\boldsymbol{\tau}_{C,i}$ acts on $\boldsymbol{p}_i$.

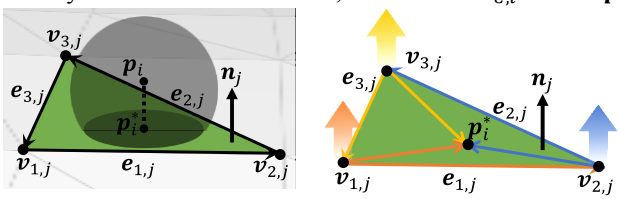

(a) $\boldsymbol{p}_i^*$ derived by projecting $\boldsymbol{p}_i$ onto m_j (b) $\boldsymbol{p}_i^*$ exists in m_j

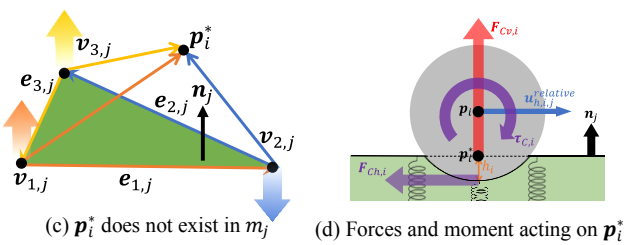

(c) $\boldsymbol{p}_i^*$ does not exist in m_j (d) Forces and moment acting on $\boldsymbol{p}_i^*$

Figure 5. Discrimination of $\boldsymbol{p}_i$ with respect to m_j and contact forces.

$$\boldsymbol{\tau}_{C,i} = (-r\boldsymbol{n}_j) \times \boldsymbol{F}_{Ch,i} \tag{13}$$

A-2. A mass point and mesh edges

If only discrimination as A-1 is used, the discrimination area of the mesh surface, such as the area above the line of convex edges (Figure 6(a)) and the area below the line of concave edges (Figure 6(b)), does not extend to the area where a mass point is not discriminated. If a mass point approaches an object from such the area, the mass point may not be discriminated and may penetrate too much into the object. So, a mass point that is discriminated as not being on or under any mesh surface in A-1 is considered to be in contact and friction with the following mesh edges. Let $\boldsymbol{p}_i^*$ be the nearest point of $\boldsymbol{p}_i$ to the mesh edge vector $\boldsymbol{e}_j$.

$$\boldsymbol{p}_i^* = \boldsymbol{v}_j + (\boldsymbol{p}_i - \boldsymbol{v}_j) \cdot \boldsymbol{t}_j \tag{14}$$

However, $\boldsymbol{t}_j$ is the unit vector of $\boldsymbol{e}_j$. $\boldsymbol{p}_i$ exists above or below the line of $\boldsymbol{e}_j$ if the following equation is satisfied for $\boldsymbol{p}_i^*$.

$$0 \le (\boldsymbol{p}_i^* - \boldsymbol{v}_j) \cdot \boldsymbol{t}_j \le |\boldsymbol{e}_j| \tag{15}$$

If $\boldsymbol{p}_i$ satisfies (15) and is on or below $\boldsymbol{e}_j$, the amount of penetration h_i of $\boldsymbol{p}_i$ into $\boldsymbol{e}_j$ is calculated (Figure 6(c) and 6(d)).

$$h_i = r - \mathrm{sgn}\{(\boldsymbol{n}_j \times \boldsymbol{n}_{j+\alpha}) \cdot \boldsymbol{e}_j\}|\boldsymbol{p}_i - \boldsymbol{p}_i^*| \tag{16}$$

Note that $\boldsymbol{n}_j$ and $\boldsymbol{n}_{j+\alpha}$ are the outward normal vectors in two adjacent mesh bounded by $\boldsymbol{e}_j$. Using (16), the vertical drag and friction forces are formulated in the same method as described in the latter half of A-1. Note that the direction of the vertical drag force is undefined because the outward normal vector $\boldsymbol{n}_j$ that the mesh has cannot be defined on the mesh edges. Thus, the direction of the vertical drag force $\boldsymbol{n}_{F,i}$ is defined.

$$\boldsymbol{n}_{F,i} = \mathrm{sgn}\{(\boldsymbol{n}_j \times \boldsymbol{n}_{j+\alpha}) \cdot \boldsymbol{e}_j\} \frac{\boldsymbol{p}_i - \boldsymbol{p}_i^*}{|\boldsymbol{p}_i - \boldsymbol{p}_i^*|} \tag{17}$$

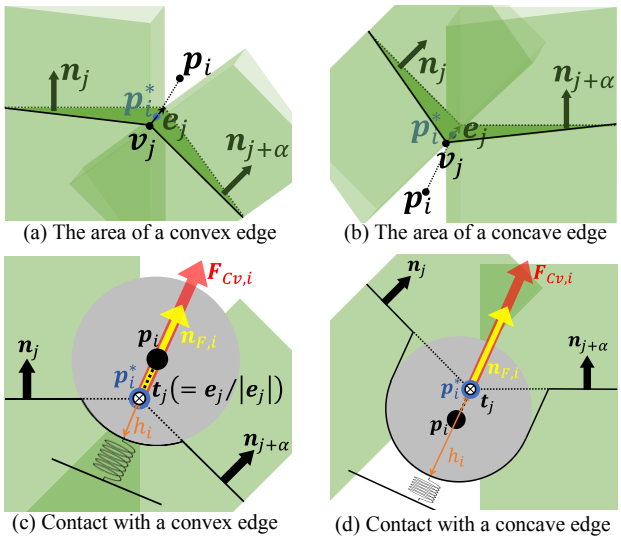

(a) The area of a convex edge (b) The area of a concave edge

(c) Contact with a convex edge (d) Contact with a concave edge

Figure 6. Discrimination of $\boldsymbol{p}_i$ with respect to $\boldsymbol{e}_j$ and contact forces.

A-3. A mass point and mesh vertices

If only discrimination as A-1 and A-2 are used, the discrimination area does not extend to regions such as the point-above area of a convex apex where all adjacent edges are

convex edges and the point-below area of a concave apex where all adjacent edges are concave edges, resulting in areas where a mass point is not discriminated. If a mass point approaches an object from such areas, the mass point may not be discriminated and may penetrate too much into the object. Therefore, a mass point that is discriminated as not existing in any area in A-1 and A-2 is considered to be in contact and friction with the following mesh vertices. The amount of penetration h_i of $\boldsymbol{p}_i$ with respect to $\boldsymbol{v}_j$ is calculated.

$$h_i = \begin{cases} r - |\boldsymbol{p}_i - \boldsymbol{v}_j| & (\boldsymbol{v}_j \text{ is a convex vertex}) \\ r + |\boldsymbol{p}_i - \boldsymbol{v}_j| & (\boldsymbol{v}_j \text{ is a concave vertex}) \end{cases} \quad (18)$$

Using (18), the vertical drag and friction forces are formulated in the same method as described in the latter half of A-1. Note that the direction of the vertical drag force is undefined because the outward normal vector $\boldsymbol{n}_j$ does not exist at the mesh vertices as well as at the mesh edges. Therefore, the direction of the vertical drag force $\boldsymbol{n}_{F,i}$ is determined.

$$\boldsymbol{n}_{F,i} = \begin{cases} \dfrac{\boldsymbol{p}_i - \boldsymbol{v}_j}{|\boldsymbol{p}_i - \boldsymbol{v}_j|} & (\boldsymbol{v}_j \text{ is a convex vertex}) \\ -\dfrac{\boldsymbol{p}_i - \boldsymbol{v}_j}{|\boldsymbol{p}_i - \boldsymbol{v}_j|} & (\boldsymbol{v}_j \text{ is a concave vertex}) \end{cases} \quad (19)$$

A-4. A straight spring and mesh edges

Straight springs as well as mass points are components of yarn, so contact and friction of straight springs are also considered. As with mass points, possible contact targets for straight springs include the mesh surface, edges, and vertices. However, when a straight spring contacts a mesh surface, if the entire straight spring is included in the mesh surface, then that case is considered in the contact of the mass points at both ends of the straight spring. If the entirety of the straight spring is not included in the mesh surface, then the contact with the edge should be considered. As for the contact and friction between the straight spring and the vertex, the vertex can be included in the contact with the edge by considering it as a point at the edge. Thus, the contact and friction between the straight spring and the edge are formulated. The contact and friction between the straight spring vector $\boldsymbol{d}_i$ connecting $\boldsymbol{p}_{i-1}$ and $\boldsymbol{p}_i$ and the mesh edge vector $\boldsymbol{e}_j$ connecting the mesh vertices $\boldsymbol{v}_{j-1}$ and $\boldsymbol{v}_j$ is considered. The nearest contact points $\boldsymbol{p}_{s,i}$ and $\boldsymbol{p}_{e,j}$ at the two vectors on each vector are formulated (Figure 7(a)).

$$\boldsymbol{p}_{s,i} = \boldsymbol{p}_{i-1} + u_i \boldsymbol{t}_i \quad , \quad \boldsymbol{p}_{e,j} = \boldsymbol{v}_{i-1} + u_j \boldsymbol{t}_j \quad (20)$$

Note that $\boldsymbol{t}_i$ and $\boldsymbol{t}_j$ are unit vectors of each vector. Also, u_i and u_j are unknowns. The vector connecting the nearest neighbor points are always orthogonal to each vector.

$$\boldsymbol{t}_i \cdot (\boldsymbol{p}_{s,i} - \boldsymbol{p}_{e,j}) = 0 \quad , \quad \boldsymbol{t}_j \cdot (\boldsymbol{p}_{s,i} - \boldsymbol{p}_{e,j}) = 0 \quad (21)$$

When derived u_i and u_j satisfy (22), $\boldsymbol{d}_i$ and $\boldsymbol{e}_j$ may contact.

$$0 \le u_i \le |\boldsymbol{d}_i| \quad , \quad 0 \le u_j \le |\boldsymbol{e}_j| \quad (22)$$

The amount of penetration h_i for $\boldsymbol{e}_j$ in $\boldsymbol{p}_{s,i}$ is formulated.

$$h_i = r - \left[\mathrm{sgn}\{\boldsymbol{n}_j \cdot (\boldsymbol{p}_{s,i} - \boldsymbol{p}_{e,j})\} + \mathrm{sgn}\{\boldsymbol{n}_{j+\alpha} \cdot (\boldsymbol{p}_{s,i} - \boldsymbol{p}_{e,j})\} + 1\right] |\boldsymbol{p}_{s,i} - \boldsymbol{p}_{e,j}| \quad (23)$$

$\boldsymbol{n}_j$ and $\boldsymbol{n}_{j+\alpha}$ are the outward normal vectors in two adjacent mesh bounded by $\boldsymbol{e}_j$. Using (23), the vertical drag and friction forces are formulated in the same method as described in the latter half of A-1. Note that the direction of the vertical drag force is undefined because there is no outward normal vector on the mesh edges as there is on the mesh planes. Therefore, the direction of the vertical drag force $\boldsymbol{n}_{F,i}$ is determined by $\boldsymbol{p}_{s,i}$ and $\boldsymbol{p}_{e,j}$. In addition, since the model of yarn is a discrete model, only the motion of masses is analyzed. Therefore, the force acting on the straight spring must be distributed appropriately to the masses at both ends of the straight spring (Figure 7(b)). If the vertical drag force generated by the i-th straight spring contacting the mesh edge is $\boldsymbol{F}_{Cv,i}^{spring}$, the vertical drag force distributed to the masses at both ends is formulated.

$$\boldsymbol{F}_{Cv,i-1}^{devided} = (1 - u_i)\boldsymbol{F}_{Cv,i}^{spring} \quad , \quad \boldsymbol{F}_{Cv,i}^{devided} = u_i \boldsymbol{F}_{Cv,i}^{spring} \quad (24)$$

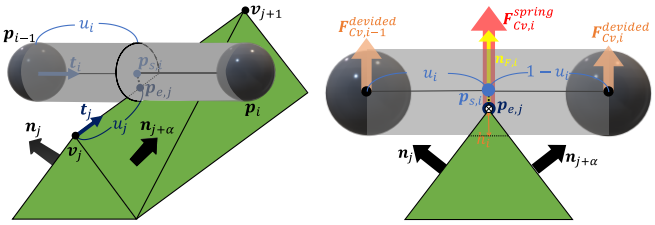

(a) Contact between $\boldsymbol{d}_i$ and $\boldsymbol{e}_j$ (b) Division of contact force

Figure 7. Discrimination of $\boldsymbol{d}_i$ with respect to $\boldsymbol{e}_j$ and contact forces.

B. Contact and friction between yarns

The yarn model in this research are composed of mass points and straight springs. Therefore, to model the contact and friction between yarns, 3 patterns of contact and friction should be considered: a mass point to a mass point, a mass point to a straight spring, and a straight spring to a straight spring.

B-1. A mass point to a mass point

For the i-th mass point $\boldsymbol{p}_i$ and the j-th mass point $\boldsymbol{p}_j$, they are in contact if the following equation is satisfied.

$$|\boldsymbol{p}_i - \boldsymbol{p}_j| \le 2r \quad (25)$$

When the masses contact each other, define the normal vector $\boldsymbol{n}_{F,i}$ to the contact surface and the amount of penetration h_i.

$$h_i = r - \frac{|\boldsymbol{p}_i - \boldsymbol{p}_j|}{2} \quad , \quad \boldsymbol{n}_{F,i} = \frac{\boldsymbol{p}_i - \boldsymbol{p}_j}{|\boldsymbol{p}_i - \boldsymbol{p}_j|} \quad (26)$$

By considering the contact surface as same as a mesh surface, the vertical drag and friction forces can be formulated in the same method as described in the latter half of A-1 (Figure 8).

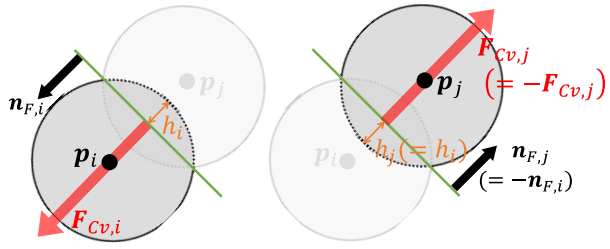

Figure 8. Contact forces due to contact between the mass points.

B-2. A mass point to a straight spring

For the i-th mass point $\boldsymbol{p}_i$ and the j-th straight spring $\boldsymbol{d}_j$, if (27) is satisfied, they contact. Note $\boldsymbol{t}_j$ is a unit vector of $\boldsymbol{d}_j$.

$$\begin{cases} 0 \le \boldsymbol{t}_j \cdot (\boldsymbol{p}_i - \boldsymbol{p}_{j-1}) \le |\boldsymbol{d}_j| \\ \left|(\boldsymbol{p}_i - \boldsymbol{p}_{j-1}) - \{\boldsymbol{t}_j \cdot (\boldsymbol{p}_i - \boldsymbol{p}_{j-1})\}\boldsymbol{t}_j\right| \le 2r \end{cases} \tag{27}$$

When they are in contact, a normal vector $\boldsymbol{n}_{F,i}$ to the contact surface and the amount of penetration h_i are defined.

$$\begin{cases} h_i = r - \dfrac{\left|(\boldsymbol{p}_i - \boldsymbol{p}_{j-1}) - \{\boldsymbol{t}_j \cdot (\boldsymbol{p}_i - \boldsymbol{p}_{j-1})\}\boldsymbol{t}_j\right|}{2} \\ \boldsymbol{n}_{F,i} = \dfrac{(\boldsymbol{p}_i - \boldsymbol{p}_{j-1}) - \{\boldsymbol{t}_j \cdot (\boldsymbol{p}_i - \boldsymbol{p}_{j-1})\}\boldsymbol{t}_j}{\left|(\boldsymbol{p}_i - \boldsymbol{p}_{j-1}) - \{\boldsymbol{t}_j \cdot (\boldsymbol{p}_i - \boldsymbol{p}_{j-1})\}\boldsymbol{t}_j\right|} \end{cases} \tag{28}$$

Using these, the vertical drag force $\boldsymbol{F}_{Cv,i}$ and friction force $\boldsymbol{F}_{Ch,i}$ acting on $\boldsymbol{p}_i$ are formulated in the same method as described in the latter half of A-1 (Figure 9(a)). Next, the vertical drag and friction forces acting on $\boldsymbol{d}_j$ are defined by the reaction of the forces acting on $\boldsymbol{p}_i$, $\boldsymbol{F}_{Cv,j}(= -\boldsymbol{F}_{Cv,i})$ and $\boldsymbol{F}_{Ch,j}(= -\boldsymbol{F}_{Ch,i})$, respectively, and the combined force is $\boldsymbol{F}_{C,j}$. The moment $\boldsymbol{M}_{C,j}$ due to frictional force are then formulated.

$$\boldsymbol{M}_{C,j} = \left\{\left(u_j^* - \frac{|\boldsymbol{d}_j|}{2}\right)\boldsymbol{t}_j + (-r\boldsymbol{n}_{F,i})\right\} \times \boldsymbol{F}_{C,j} \tag{29}$$

Note that u_j^* is the distance from the starting point of $\boldsymbol{d}_j$ to the point of contact, and is formulated as (30).

$$u_j^* = \boldsymbol{t}_j \cdot (\boldsymbol{p}_i - \boldsymbol{p}_{j-1}) \tag{30}$$

The forces and moments acting on the straight spring must be distributed to the masses at both ends of the spring. In general, when a force acts on a rigid body at a certain distance from the centroid, it is equivalent to the force and the moment caused by the force acting on the centroid. Therefore, it is assumed that the moment caused by the vertical drag force, frictional force, and frictional force is applied to the centroid of yarn, and it is considered to distribute them to the mass points at both ends. Thus, for considering distribution of forces and moments, $\boldsymbol{\beta}_j$ is newly defined. The tangential direction of the line segment is $\boldsymbol{t}$ direction, the normal direction of the contact surface is $\boldsymbol{n}_F$ direction, and as $\boldsymbol{\beta}_j$ direction orthogonal to them.

$$\boldsymbol{\beta}_j = \frac{\boldsymbol{t}_j \times \boldsymbol{n}_{F,j}}{|\boldsymbol{t}_j \times \boldsymbol{n}_{F,j}|} \tag{31}$$

By using this coordinate $\mathrm{P} - tn_F\beta$, the calculated forces are projected to the spatial coordinate with respect to the forces and to the object coordinate with respect to the moments. As a result, the forces and moments are formulated (Figure 9(b)).

$$\begin{cases} \boldsymbol{f}_{C,j-1} = \left(1 - \dfrac{u_j^*}{|\boldsymbol{d}_j|}\right)\boldsymbol{F}_{C,j} - \dfrac{r}{|\boldsymbol{d}_j|}(\boldsymbol{F}_{Ch,j} \cdot \boldsymbol{t}_j)\boldsymbol{n}_{F,j} \\ \boldsymbol{f}_{C,j} = \dfrac{u_j^*}{|\boldsymbol{d}_j|}\boldsymbol{F}_{C,j} + \dfrac{r}{|\boldsymbol{d}_j|}(\boldsymbol{F}_{Ch,j} \cdot \boldsymbol{t}_j)\boldsymbol{n}_{F,j} \end{cases} \tag{32}$$

$$\begin{cases} \boldsymbol{m}_{C,j-1} = \left(1 - \dfrac{u_j^*}{|\boldsymbol{d}_j|}\right)\{(-r\boldsymbol{n}_{F,j}) \times (\boldsymbol{F}_{Ch,j} \cdot \boldsymbol{\beta}_j)\} \\ \boldsymbol{m}_{C,j} = \dfrac{u_j^*}{|\boldsymbol{d}_j|}\{(-r\boldsymbol{n}_{F,j}) \times (\boldsymbol{F}_{Ch,j} \cdot \boldsymbol{\beta}_j)\} \end{cases} \tag{33}$$

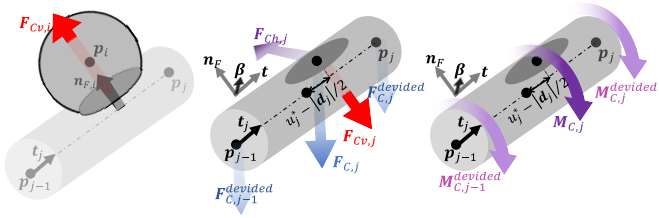

(a) Contact force on $\boldsymbol{p}_i$ (b) Contact force on $\boldsymbol{d}_i$ and dividing it

Figure 9. Contact forces due to contact between $\boldsymbol{p}_i$ and $\boldsymbol{d}_i$.

B-3. A straight spring to a straight spring

For the i-th straight spring $\boldsymbol{d}_i$ and the j-th straight spring $\boldsymbol{d}_j$, it is determined whether the two straight springs contact using the two-line contact determination described in A-4. If they are determined to be in contact, the following variables are defined.

$$\begin{cases} h_i = r - \dfrac{\boldsymbol{n}_{F,j} \cdot (\boldsymbol{p}_{i-1} - \boldsymbol{p}_{j-1})}{2} \\ \boldsymbol{n}_{F,i} = \mathrm{sgn}\left\{(\boldsymbol{p}_{i-1} - \boldsymbol{p}_{j-1}) \cdot \dfrac{\boldsymbol{t}_i \times \boldsymbol{t}_j}{|\boldsymbol{t}_i \times \boldsymbol{t}_j|}\right\} \dfrac{\boldsymbol{t}_i \times \boldsymbol{t}_j}{|\boldsymbol{t}_i \times \boldsymbol{t}_j|} \end{cases} \tag{34}$$

These are used to calculate the vertical drag and friction forces. Note that since this is contact between straight springs, which must be distributed to the mass points at both ends, contact and friction between straight springs can be formulated by making the same distribution as described in the latter half of B-2.

V. Case Study

Based on the modeling presented above, a simulation of yarn knitted on a knitting machine is performed. Parameters in this simulation are shown in Table 1.

TABLE I. Parameters in this simulation.

Line density	5.6×10^{-3}[mg/mm]
Radius of a mass point	4.0×10^{-2}[mm]
Length of a segment	0.10[mm]
Constant of contact spring	1.0×10^{3}[N/m]
Elongational rigidity	6.6×10^{3}[N]
Flexural rigidity	4.7[N · m^2]
Torsional rigidity	1.5[N · m^2]
Coefficient of static friction	0.50
Coefficient of kinetic friction	0.30

Additionally, contact patterns between yarn and a knitting machine is numerous as described in this paper, making contact calculations too complex. Furthermore, since multiple knitting machine parts with complex curved surface shapes are used in the simulation, the number of mesh surface for which contact calculations are performed for yarns becomes large. Therefore, the computation time is expected to increase. Thus, this simulation uses BVH [8], which is a simulation acceleration method, to perform calculation efficiently. This method achieves speedup by omitting calculations in areas where contact is unlikely. By using this, the computation time for this was approximately 8 hours. Without this, the computation time was not even completed in about one week. Based on the result, the computation was made about 20 times more efficient. However, the degree of this effect is for this case study, and the impact of this effect will increase as the number of meshes increases.

A frame-by-frame movie of the simulation result is shown in Figure 10. The left side of each figure shows the front view and the right side shows the right side view. The parts that are moving vertically as the simulation progresses are knitting machine needles, and the parts that are not moving are fixed sinkers. By controlling these parts, yarn is knitted to form a knitted fabric. In this figure, these parts are drawn transparently so that the yarn in the process of being knitted can be easily seen. In addition, the part that is present at the top of each figure in Figure 10 is called the feeder, which is the part that supplies new yarn. As can be seen from this figure, the yarn fed from the feeder is knitted while making intermittent and repeated contact with the needles and fixed sinkers. In addition, this yarn is simulated in contact with other yarns present at the bottom of each figure in Figure 10. Furthermore, normal strain in each straight spring at 40[msec], the end time of the simulation, is shown in Figure 11. As can be seen from this figure, there is an asymmetry of the normal strain on the left and right sides of each loop, bounded by the central axis of each needle indicated by dotted lines in the figure. In other words, the knitted fabric after immediately knitting has the asymmetry of the normal strain. It is considered that this asymmetry of normal strain occurring within the loop is homogenized, resulting in the loop to tilt. This is probably what has led to the occurrence of Yotari. From the above, this simulation verified whether the hypothesis on the occurrence of Yotari can actually occur as a phenomenon.

VI. Conclusion

The final goal of this research is to predict the occurrence and investigate the cause of Yotari. It is considered that the interaction of contact and friction between the knitting machine and yarn, or yarns during the knitting process has a significant effect. Therefore, these phenomena are modeled faithfully in this paper. By the proposed method, yarns knitted on a knitting machine are simulated to reproduce the phenomena that would occur in Yotari. In the future, the proposed method will be compared with experiments to demonstrate its validity and to achieve the final goal.

References

[1] Christine Snedker, “Knitted objects: Exploring flat knitting as a technique to design form”, Faculty of Textiles, Engineering and Business, 2019, pp. 1-46

[2] Hong Hu, Zhengyue Wang, Su LiuView, “Development of auxetic fabrics using flat knitting technology”, Textile Research Journal, 2011, Volume 81, Issue 14, pp. 1493-1502

[3] Jonathan M. Kaldor, Doug L. James, Steve Marschner, “Simulating knitted cloth at the yarn level”, ACM Transactions on Graphics, 2008, Volume 27, No. 3, pp. 65:1-65:9

[4] Cem Yuksel, Doug L. James, Steve Marschner, “Stitch Meshes for Modeling Knitted Clothing with Yarn-level Detail”, ACM Transactions on Graphics, 2012, Volume 31, Issue 4, No. 37, pp. 1-12

[5] Kazuki Hayano, Hidefumi Wakamatsu, Yoshiharu Iwata, and Yuya Yamada, “Dynamic Behavior Analysis of Yarns During Knitting Process of Fabrics”, Proceedings of the International Symposium on Flexible Automation 2024, Paper No. ISFA2024-140855

[6] J. C. Butcher, “Runge-Kutta methods: some historical notes”, Applied Numerical Mathematics, 1996, Volume 22, Issues 1-3, pp. 113-151

[7] J. Baumgarte, “Stabilization of constraints and integrals of motion in dynamical systems”, Computer Methods in Applied Mechanics and Engineering, 1972, Volume 1, Issue 1, pp. 1-16

[8] M. Ernst, G. Greiner, "Multi bounding volume hierarchies", IEEE Symposium on Interactive Ray Tracing, 2008, pp. 35-40

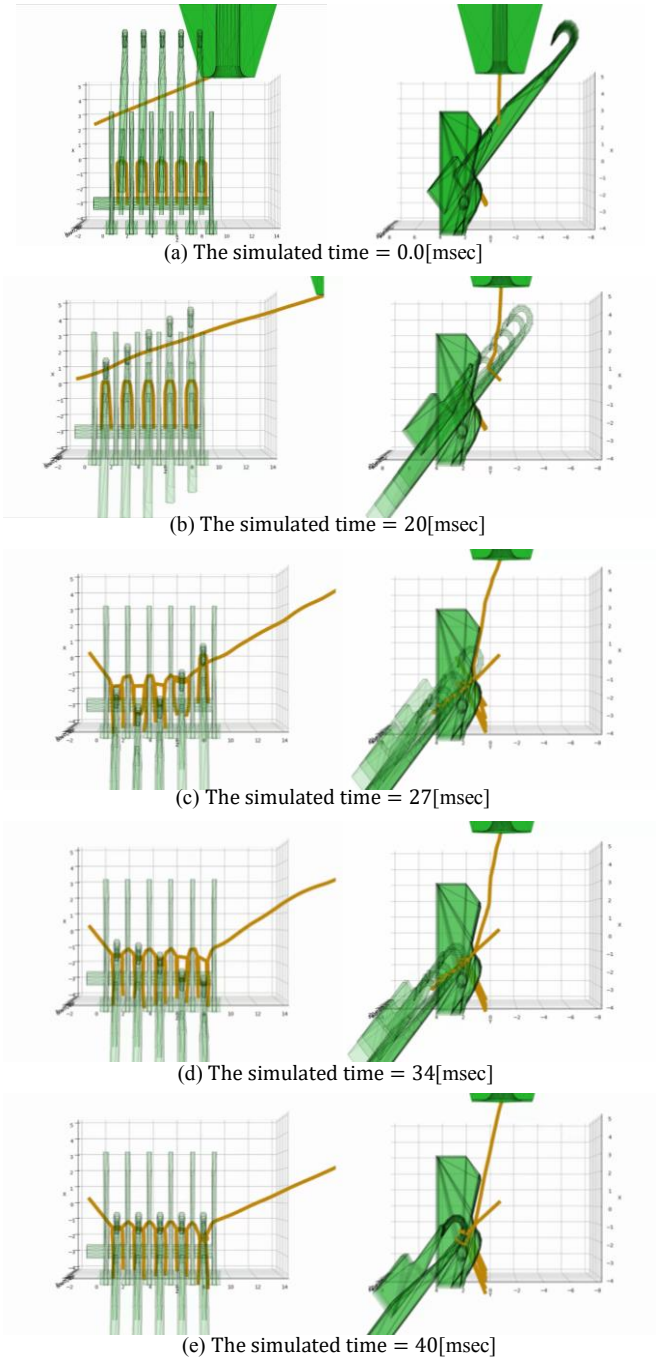
(a) The simulated time = 0.0[msec]

(b) The simulated time = 20[msec]

(c) The simulated time = 27[msec]

(d) The simulated time = 34[msec]

(e) The simulated time = 40[msec]

Figure 10. Dynamic simulation results of knitting process.

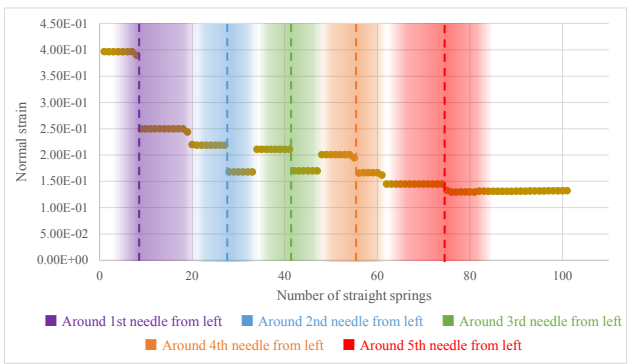

Figure 11. Normal strain of each straight spring at 40 msec.